Tidal Tails of Interacting Galaxies

Timothy Harrison

March 2011

Abstract

A computer simulation of two galaxies, passing in parabolic orbits, was made to show their interaction and the tidal patterns formed. The galaxies were modelled as a point masses surrounded by 5 densely packed, concentric rings of test masses in circular motion, which represented the outer disk of the galaxy. Several features were noticeable in the simulations, including: a bridge forming between the two galaxies during the interaction, mass being lost to the perturbing galaxy and universe, and an arching *counterarm* emanating away from the bridge. The results suggest the process was primarily kinematic. Quantitative analysis was made on the *counterarm length* dependence on galaxy separation and mass ratio. In both cases linear relationships were found with arm length increasing for smaller separations and for larger perturbing masses. The effects were greatly reduced in a retrograde interaction. The images were compared to astrophysical observations and qualitative features matched.

1 Introduction

The passing and merging of galaxies and its likelihood of occurrence has been studied by the scientific community since 1940[1]. In 1941 Holmberg discussed in [2] how these interactions would cause large tidal disturbances. He obtained quantitative estimates of the energy lost using an analog computer with 74 movable lamps representing 37 bodies per galaxy. Unfortunately, over the next 30 years very little progress was made, mainly because most believed these interactions to be very rare events, as was supported by simple order of magnitude estimates of their probability[3]. During the 1970s, however, several arguments[4] arose suggesting the events were much more common and Toomre's observational evidence in [5] found an unpredicted proportion of galaxies in "fairly advanced throes of merger".

The problem of simulating an interaction is inherently non-analytic due to the large number of bodies involved. Fortunately, by the 1970s advances in computational power and numerical methods meant lightbulbs were no longer necessary. The work of Toomre & Toomre [6] modelled the galaxies as point masses surrounded by concentric rings of test masses representing the outer disks. Full N-body simulations were conducted by White, Roos & Norman and Dekel et al. in [7, 8, 9] respectively, with up to 250 bodies per galaxy. Models expanding the perturbing potential in a set orthogonal functions and keeping lowest order terms have been used for their greater efficiency. These have been performed by Villumsen and Miller & Smith in [10, 11] with up to 50,000 bodies per galaxy - although small scale features were lost[3]. With further advances in computers, the numbers of bodies in each type of simulation continues to increase.

The evidence that these tidal effects occur in our universe is supported by observational evidence of several galaxies[6], for example Arp 242 and Arp 244, which qualitatively match many results

of the simulated features. It should be noted that there is observational evidence which does not match so well with simulations, for example the galaxy NGC 2535. It has been suggested these discrepancies may be due to magnetic or viscous effects as well as peculiar orbits [6, 13]. The importance of this subject is highlighted by this observational evidence, which suggests it is a phenomenon that occurs in our universe. By performing ever better simulations one can test how well our model matches data and extend the model to include other effects.

In this computational project a parabolic orbit interaction between two galaxies with massless particles constituting the outer disk was made in a set up very similar to that of Toomre & Toomre in [6]. Qualitative observations are made of the general process under several different starting conditions and a quantitative investigation is made into the lengths of the tidal tails for different set ups. The computational analysis and relevant theory is put forth in Section 2 and the implementation and performance of the code is described in Section 3. Section 4 contains the results and discussions (including tests to ensure accuracy of results) and Section 6 contains the overall conclusions.

2 Computational Analysis

The interacting galaxies are modelled as point masses surrounded by rings of non-interacting test masses. These rings represent the stars/medium in the outer disc of the galaxy; however, it is clearly inaccurate that we model the outer disc as massless. Nevertheless, assuming that the majority of a galaxy's mass is central and that self attraction of outer parts of the galaxy is small, the model should provide reasonable results. Primarily it should be noted that it is vastly more efficient than a full N-body ($\mathcal{O}(N^2)$) calculation which also suffers more from statistical fluctuations[3] (due to the smaller number of bodies used) and two-body relaxation effects (Appendix A).

The problem is simply a classical many-body system under the effects of Newtonian gravity. There are of course many possible algorithms, most notably the 4^{th} order Runge-Kutta scheme and the Verlet algorithm. Both methods provide accuracy of ($\mathcal{O}(\tau^4)$), where τ is the time increment used, and are relatively simple to code. Here the Verlet algorithm was chosen due to its time reversibility and for being symplectic[1], making it highly advantageous for long-term evolution of many body systems.

The Verlet Algorithm is formulated by applying a three point formula to the second order derivative $\frac{d^2\mathbf{R}}{dt^2}$, where $\mathbf{R}$ represents the coordinates $(\mathbf{r}_1, \mathbf{r}_2, ..., \mathbf{r}_N)$ and t is time. If $\mathbf{G}$ and $\mathbf{V}$ represent the vector accelerations and velocities of the particles it can be shown that (see [12]) :

$$\mathbf{R}_{k+1} = 2\mathbf{R}_{k+1} - \mathbf{R}_{k-1} + \tau^2\mathbf{G}_k + \mathcal{O}\left(\tau^4\right) \tag{1}$$

$$\mathbf{V}_k = \frac{\mathbf{R}_{k+1} - \mathbf{R}_{k-1}}{2\tau} + \mathcal{O}\left(\tau^2\right) \tag{2}$$

This algorithm predicts the position and velocity at step number k (with $t = k\tau$) and can be started if the first two positions of all bodies are given. In practice, the positions $\mathbf{R}_1$ are calculated from the initial conditions ($k = t = 0$) by treating the force as constant over the initial time step:

[1] A symplectic integrator possesses a Hamiltonian, which is slightly perturbed from the original, as a conserved quantity.

$$\mathbf{R}_1 \simeq \mathbf{R}_0 + \tau \mathbf{V}_0 + \frac{\tau^2}{2}\mathbf{G}_0 \tag{3}$$

This procedure can easily be improved by performing the Taylor expansion to higher order terms and replacing $\mathbf{G}_0$ with an average force over the first time interval. Using the algorithm, the position calculation requires no information on the calculated velocity whose error is two orders of magnitude higher. Where velocity isn't necessary, its evaluation can be ignored. Furthermore, velocity is evaluated one time step behind the position, which is inconvenient. This lag can be removed by evaluating the velocity from the force, as derived in [12], giving:

$$\mathbf{R}_{k+1} = \mathbf{R}_k + \tau \mathbf{V}_k + \frac{\tau^2}{2}\mathbf{G}_k + \mathcal{O}\left(\tau^4\right) \tag{4}$$

$$\mathbf{V}_{k+1} = \mathbf{V}_k + \frac{\tau}{2}\left(\mathbf{G}_{k+1} + \mathbf{G}_k\right) + \mathcal{O}\left(\tau^2\right) \tag{5}$$

which is a much more useful form when velocities are wanted. Both these algorithms are implemented in the program to allow for different data to be collected efficiently in the simulation (see Section 3).

The general initial conditions required to put two bodies (of different masses) in parabolic orbit with one another with a specified separation at closest approach were also needed. The derivation is algebraically tedious although it simplifies in certain conditions. It is derived in Appendix B and implemented as described in Section 3.

The scaling of the problem was chosen to simplify the equations and keep the numbers stored in **double type** close to order 10^0 to 10^2 to maximise accuracy. The value of the gravitational constant G was set to 1 and so was the mass, M, of one of the galaxies (the other mass then took a value that gave its mass relative to M). To attain SI units from the data calculated one can multiply by GM or $\sqrt{GM}$ for distances and velocity respectively (replacing M with the reduced mass as necessary).

3 Implementation and Performance

3.1 Implementation: an Object-Oriented Approach

The code for this project was written in a fully object-oriented fashion and the full code listing can be seen in Appendix C. The advantages of object-oriented programming are well documented[14, 15]. Primarily the ease of reusability and abstraction allows one to create different initial setups and implement multiple algorithms much more neatly. The code was written to allow for any setup with an arbitrary number of galaxies and test masses.

The code, written entirely in C++, contained three classes, all of which implemented a fourth which represented a two dimensional vector (**Vec2**[2]). The class **CTestMass** represents a test mass or star in the outer ring of a galaxy. It has obvious properties including: **Vec2** objects for position, velocity, acceleration and their values at the last step in the algorithm. The class **CGalaxy** represented the point mass at the centre of galaxy and was a sub class of

[2]The class **Vec2** is a modified version of the **Vector** class in the **CavLib** library. It was modified to be for 2 dimensions and to print more appropriately for data plotting

CTestMass, which adds the property of mass (stored as a double). Wherever possible, objects were passed by reference to maximise efficiency and stored as constant, where appropriate, to minimise bugs.

CTestMass implements accessor and mutator methods to allow properties to be obtained and changed. This technique means the implementation of our class can be changed without affecting other code that uses it. This class also implements methods to perform steps for the Verlet and velocity Verlet algorithm as in Equations 1-5. Importantly, the function **updateAcceleration** takes a vector of pointers to **CGalaxy** objects and calculates the acceleration on a test mass due to them. This virtual function is overwritten in **CGalaxy** to prevent a galaxy trying to calculate the acceleration due to itself. It works for an arbitrary number of **CGalaxy** objects.

The third class **CUniverse** stores all other objects and performs the simulations. τ is stored as a **double**. References to galaxies and test masses are stored in the vectors **allGalaxies** and **allTestMasses** and simulations are performed by iterating over these objects in turn and performing the necessary updates and calculations. Several simulation methods were implemented that display different information in different formats or use different algorithms. An appropriate destructor was made for this class to ensure all objects it referenced were removed when it was destroyed. Within the file **universe.cpp** several functions are defined that create universes with different setups. The initial set up will never be the most time-demanding aspect of the program, hence, ease of use and adaptability were preferred in these functions. For example, one function created two galaxies of user defined mass, separation and starting position and put them in parabolic orbit. Another function was then able to add a ring or multiple rings of test masses around all, or specific, galaxies.

3.2 Performance

With object-oriented programming there is, undeniably, a slight penalty on performance in comparison to a procedural method. This was minimised by inlining[3] suitable methods of the classes **CGalaxy** and **CTestMass**, which removes the cost of the function call. In all methods where calculated variables were needed multiple times they were stored in temporary variables to avoid unnecessary repeat calculations. The simulation is $\mathcal{O}(N^2)$, where N is the number of galaxies and $\mathcal{O}(M)$, where M is the number of test masses. Fortunately, in this project only two galaxies are used and hence their effect on performance is fixed and insignificant compared to the 1200 test masses used. Figure 1 shows this $\mathcal{O}(M)$ relationship and highlights the differences when the velocity Verlet algorithm is used, when the code is inlined and when the data is written to file.

[3]Inlining functions instructs the compiler to insert the complete body of the function wherever it is used in the code. It can reduce the function calling overhead and is very appropriate for a lot of the small functions in **CTestMass** and **CGalaxy**. Which functions should be inlined was determined by trial and error to get the fastest run time. Further advantages include: dead code optimisation, increased locality of reference and saving on return overhead.

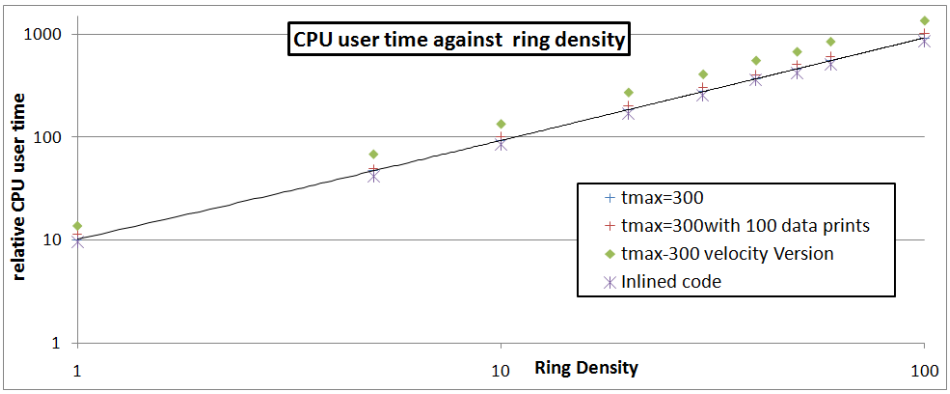

Figure 1: This graph shows the CPU time for a simulation of a specific ring density under various conditions. All times are relative to a zero test mass simulation (which took 0.005 seconds). The inlined code gave an improvement in run time of 5-7% and using the velocity version of the Verlet algorithm took longer (40-50%), as would be expected. The cost of writing the data was insignificant. The number of test masses is the ring density multiplied by 20. All test were run consecutively on the same day to minimise variations due to the PWF system.

Furthermore, the run time is proportional to the total number of steps, meaning it is $\mathcal{O}(1/\tau)$. However, the error in position in a single step is $\mathcal{O}(\tau^4)$ and so there is an upper limit on τ to minimise error as well as a lower limit to ensure feasible run time and floating point representation problems for very small τ. A test was run by placing a body in circular orbit and seeing its deviation from its analytically predicted position after 300 units of time. The results for different τ can be seen in Figure 2. For $\tau < 10^{-3}$ the relative error is $\mathcal{O}(10^{-9})$ which is significantly smaller than our plotting resolution. For most simulations done in this experiment $\tau = 0.05$ was used with a relative error $\mathcal{O}(10^{-5})$. It should be noted that a decrease in τ gives a linear increase in CPU time with a much higher power reduction in relative error. Comparisons of images were made between $\tau = 0.05$ and $\tau = 10^{-3}$. The only significant difference was when test masses were very near the centre of the galaxy, at which point modelling the galaxy as a point mass is no longer valid.

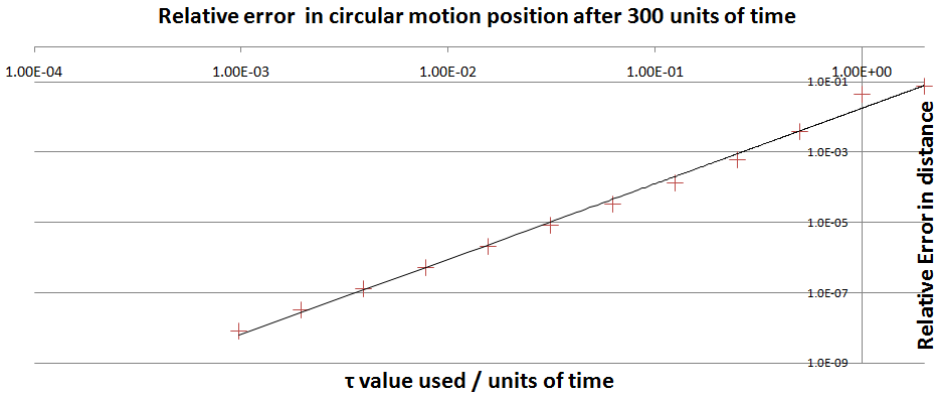

Figure 2: This graph shows the relative error in position of a singles test mass after being placed in a circular orbit about a galaxy for 300 units of time (the time for most parabolic orbits). Note the logarithmic scale. This graph can be used to estimate the value of τ needed for a required level of accuracy. $\tau = 0.05$ was used to give a relative error of $\mathcal{O}(10^{-5})$.

It was also noted that by the symmetry of the problem only one galaxy needed to be surrounded by test masses[6], reducing the run time by a factor of 2. Many other techniques were used to improve performance within the code; however, readability and simplicity were often prioritised. See the comments in the code listing (Appendix C) for more information.

4 Results and discussion

4.1 Tests Performed to Ensure Correctness

With a program containing multiple files and classes it is important to run tests on all levels of the program. Small level tests, to ensure individual functions were performing correctly, were done as the code was written. Several tests were performed to show that the program matched analytic solutions and to ensure that our initial conditions were set correctly.

4.1.1 Circular Motion Test

Using the functions **makeRingSystem** in **universeClass.cpp** and a constructed **CUniverse** object it was simple to create a set of test masses in rings in circular motion about a galaxy with arbitrary position and velocity (it was important to include the effects of the galaxy's motion!). The results can be seen in Figure 3 which shows the test masses are still accurately in circular motion after 1000 units of time.

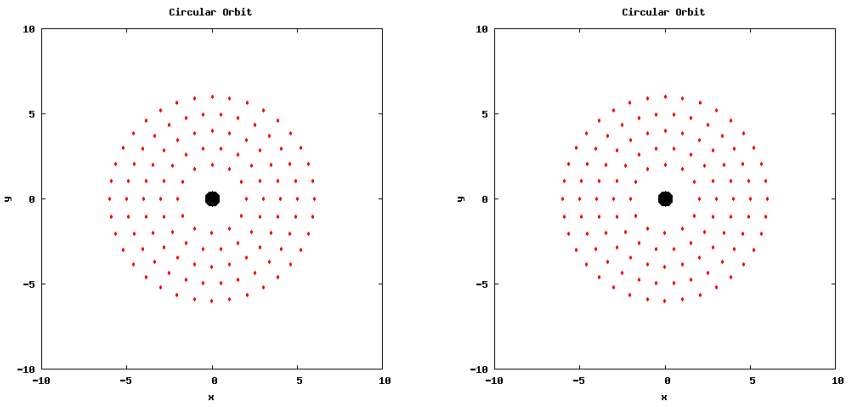

(a) t=0 (b) t=1000

Figure 3: This shows the position of a stationary galaxy (black dot) surrounded by 120 test masses (red) orbiting in circular motion. They are still in stable orbit after 1000 units of time, as expected analytically. This time length is far longer than any simulation run. A similar test was conducted for a galaxy with an initial velocity and similar results were seen.

4.1.2 Intergalactic Interaction: Two-Body Problems

It was then necessary to test that galaxies were interacting correctly with one another. For this project only two galaxies were used and so 2-body tests were the focus. Using the analytically

calculated initial conditions (Appendix B) galaxies were put in parabolic orbit with one another and their orbits could be compared with analytic results as shown in Figure 4.

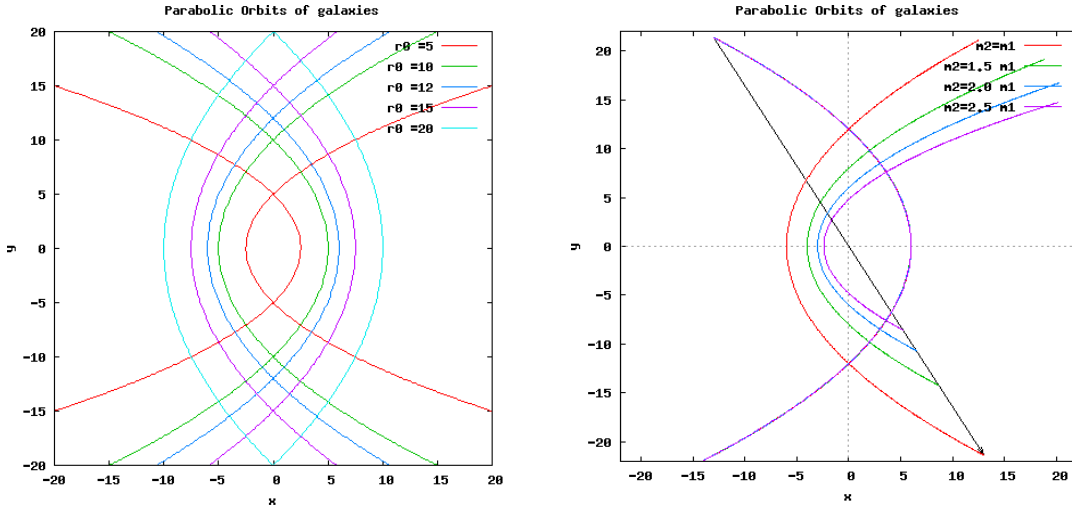

(a) Different Separations

(b) Different Masses

Figure 4: These figures show that the calculated positions of galaxies set in parabolic orbit match the theoretical predictions accurately over the length of time considered in this project. The galaxy positions were plotted at increments in the simulation and connected with lines. This, with the results shown in Figure 3, provides strong support that our results in 5 will be accurately in accordance with classical mechanics.

5 Galaxy-Galaxy Interactions: Results and Discussion

A value of $\tau = 0.05$ was used for the results in this section. In 1972 Toomre & Toomre [6] had computational power to have a ring density of 6. Thankfully, improvement in technology means we can easily use ring densities much larger (a ring density of 60 was used), allowing us to get a much clearer image of the structure during the interaction. The simulation was always started at a distance large enough that the effect of the second galaxy was initially negligible. This can bee seen by the fact the circular motion of the test masses is not initially perturbed.

5.1 A General Simulation: same mass, separation 12 units

Some interesting general features of the tidal interactions are worth discussing before we change the initial conditions and perform a more quantitative investigation. During the interaction a thin transient bridge (Figure 5d) is formed between the two galaxies from the tidal tail. It has almost disappeared after a short interval (5e); however, the counter arm remains for much longer but is eventually lost. By using a much higher ring density, the resolution of the bridge is greatly improved and one sees how it raps around the second galaxy - this structure was not visible in [5, 6]. The most central ring is mainly unaffected. When test mass positions are very close to the galaxy the results are inaccurate. This is because the force will become extremely large and errors in the Verlet algorithm, as well as errors due to floating point representation, will become significant. Furthermore, modelling the galaxy as a point mass is invalid for test

masses so close to the centre. But this shouldn't affect the overall discussion. It is also noted that the second galaxy takes away material from the first (a process that can lead to galactic cannibalism [13]) and that a small proportion of test masses are unbound from both galaxies after the interaction.

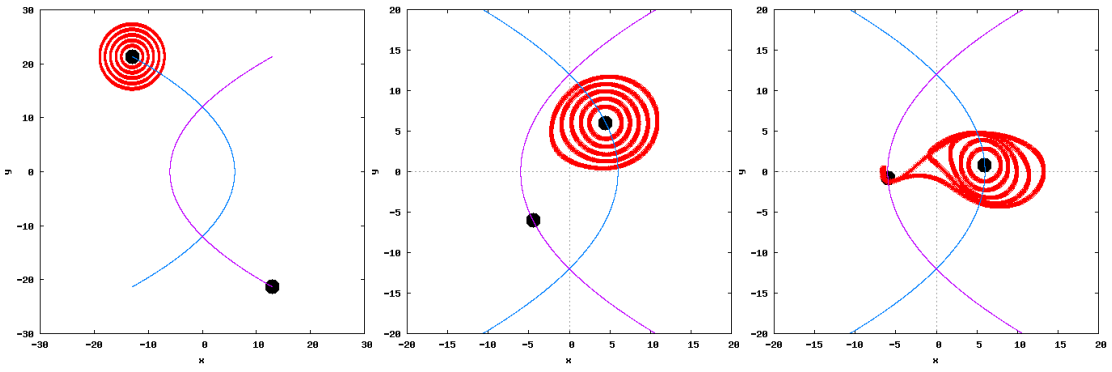

(a) t=0 (b) t=130 (c) t=150

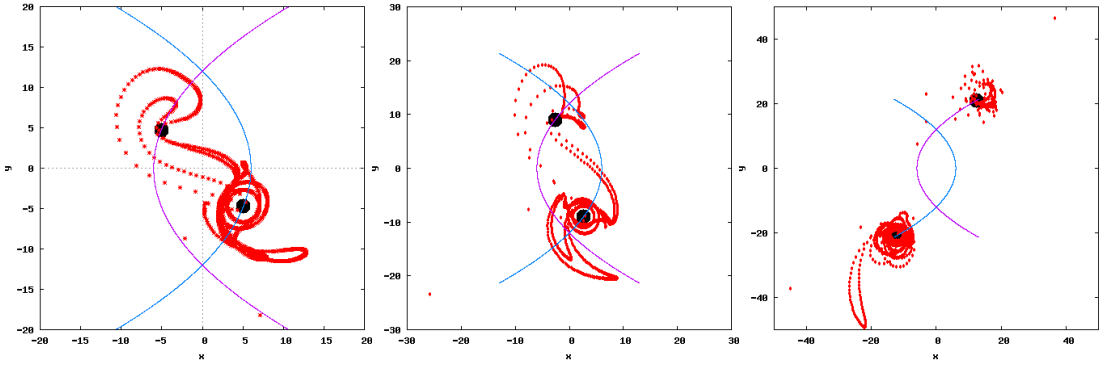

(d) t=170 (e) t=190 (f) t=300

Figure 5: The progression of a galaxy with ring density 60 is shown at 6 different stages over a simulation that lasted 300 units of time. The separation of galaxies at closest approach is 12 units and the start position of the galaxies is $r = 25$. No significant deviation is visible till $t = 130$. A tidal tail forms a bridge to the second galaxy and a counterarm is formed and extends away from it. At large times the tidal pattern is lost.

5.2 Variation of Separation at Closest Approach

In this section the effects of varying the separation at closest approach is investigated. Of course, if the galaxies are made to pass too close the model is invalidated as we can not ignore self gravity effects as galaxies overlap. Simulations were run for separations from 5 to 15 units in increments of 1 unit and a selection of the results during the violent stage of the interaction are shown in Figure 6. The closer separations have a much more violent interaction with many more test masses lost to the second galaxy and universe. The counterarm's length gets smaller as separation increases. This is because the process of formation of these arms is largely kinematic [1, 5, 6, 13] and the closer the galaxies are, the faster they will be moving relative to each other when interacting, leading to a longer arm. This effect is examined quantitatively in Figure 7 by measuring the *counterarm length* using the image analysis tool *ImageJ*. The relation between

counterarm length and separation shows a strong linear relationship supported by the linear regression performed. The relationship doesn't work well for large separations as it becomes hard to measure such small arms. The effects penetrate much deeper into the galaxy at closer separation due to the larger perturbing force.

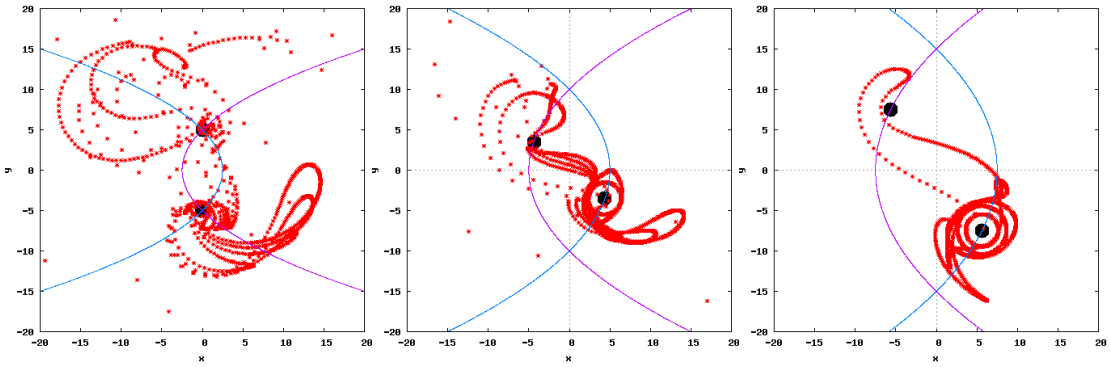

(a) separation = 5, t=150 (b) separation = 5, t=160 (c) separation = 5, t=190

Figure 6: A selection of images from galactic interactions at different separations. The times were chosen when the galactic tails were large and still well-structured. The interactions are much more violent and longer arms are formed at closer separation.

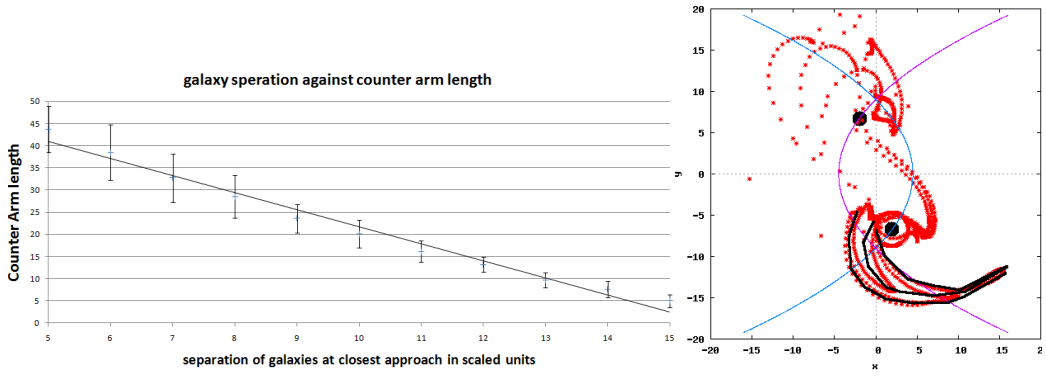

(a) results (b) method

Figure 7: The graphs show how the maximum arm length in the interaction varies with separation. It shows a strong linear correlation with gradient -3.9 ± 0.2 and intercept 60 ± 2 found from linear regression. The points do not fit the line well at large separation. The calculations for *counterarm length* for 7a were done from images such as 7b. Line segments were drawn over the image along the arm (with lines along the edges to provide upper and lower bounds to the measurement) from the start of the arm to the tip to give an estimate of its length. The *ImageJ* measurement was calibrated to the scale of the image which was kept in a 1:1 aspect ratio.

5.3 Variation of Mass of one Galaxy

In this section we examine the effects of varying the mass of one galaxy. Again a selection of images from the most violent part of the interaction is shown in Figure 8 and a quantitative examination of *counterarm length* for various masses is shown in Figure 9. The mass of the

second galaxy was fixed at 1 and the ratio of the second to the first's mass was defined as μ. For different masses to remain in parabolic orbit the separation must change but variation will be small for small masses.

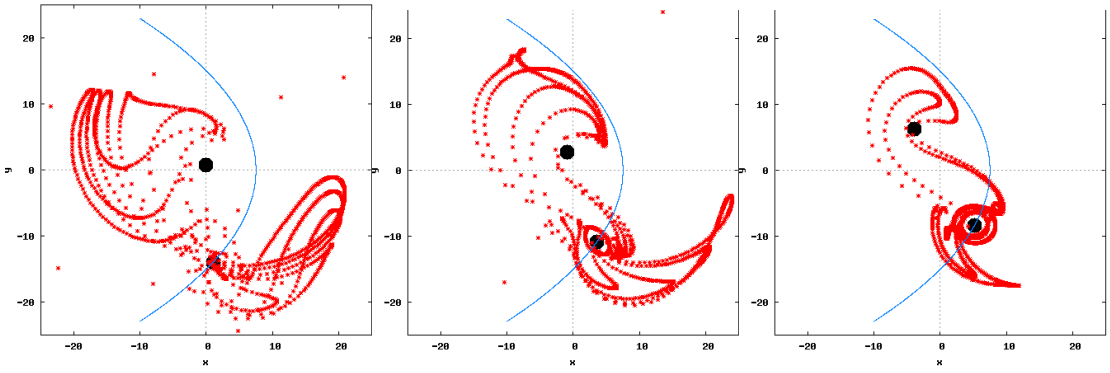

(a) mass = 0.05, t=120, $\mu = 20$ (b) mass = 0.25 = 5, t=130, $\mu = 4$ (c) mass = 0.75, t=170, $\mu = 1.33$

Figure 8: Parabolic orbit of galaxies of different masses is no longer symmetric about y axis.

It is clear from these images that when μ is large the first galaxy is disturbed much more greatly and the second galaxy rips off a much larger amount of its surrounding disc. This is to be expected as the force on the test masses is greatly dominated by the second galaxy during the interaction. The length of the arm formed, again measured using *ImageJ*, was compared to the mass (Figure 9). Again we see a linear trend with gradient -21 ± 3 showing how the *counterarm length* increases as mass decreases. The higher μ the more violent the interaction and the deeper the disturbance penetrates into the galaxy.

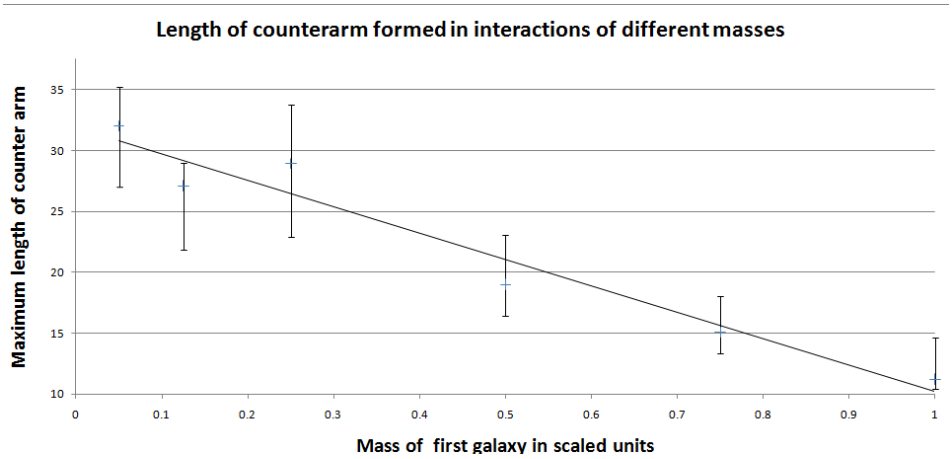

Figure 9: This graph shows how the *counterarm length* varied for different masses of the passing galaxy. The mass of the perturbing galaxy was kept at 1. A linear trend is seen with gradient -21 ± 3. The fit is not as good as Figure 7 as seen by the higher relative error in the gradient.

5.4 Retrograde Passage

As a final example, the effect of changing the sense of rotation of the test masses about the galaxy was investigated. The result was a dramatic reduction in the tidal pattern formed (compare Figure 5 to Figure 10). This dramatic reduction in tearing away test masses from the first galaxy is because there is no longer the near-resonance of orbital speeds and angular momentum of the companion galaxy[6], which created such magnificent tidal tails in prograde simulations.

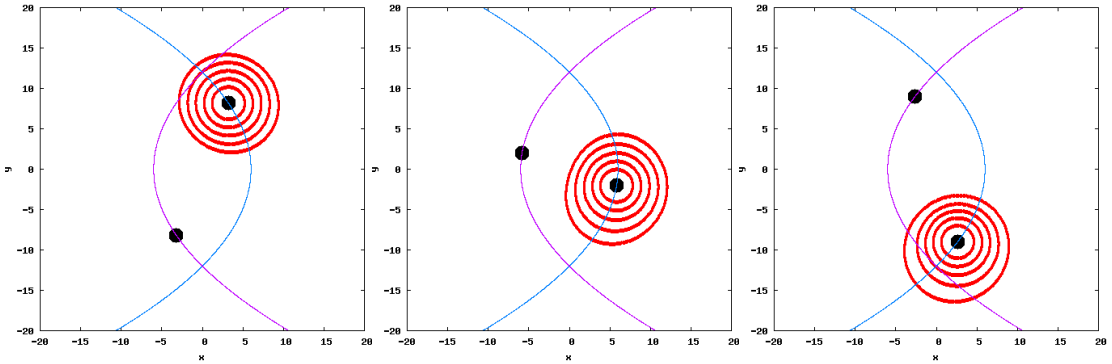

(a) t=120 (b) t=160 (c) t=190

Figure 10: A selection of images from a retrograde interaction (sense of rotation of test masses about galaxy changed with respect to Figure 5). Note that the disturbance has much less effect. These images should be compared with Figure 5.

6 Conclusion

This computational project modelled the passing or merging of two galaxies, in parabolic orbit with one another, under various conditions and analysed the tidal patterns formed. The galaxies were modelled as point masses surrounded by concentric rings of massless test particles that represented the outer disk of the galaxy. In many astronomical cases the majority of a galaxy's mass is central[16, 17] and the self gravitating effects of the outer disks are negligible in comparison. This validates our model which is much more efficient than an N-body calculation.

The simulations shows that the process of formation of tidal tails is primarily kinematic, highlighted by the patterns still changing after the range of perturbing forces are significant. The patterns formed have a characteristic form with a *bridge* forming between the two galaxies and an arching *counterarm* emanating in the opposite direction. The interaction also causes the primary galaxy to lose a proportion of its mass to the perturber and some material is lost to the universe. The amount lost increases for smaller separations and larger perturbing masses as would be expected due to the larger forces involved. A quantitative investigation into the length of the *counterarm* was done using image analysis tools and a strong linear trend was seen between separation of the galaxies at closest approach and *counterarm length*. The relation between perturbing mass and *counterarm length* also appeared approximately linear, with the *counterarm* of the less massive galaxy being significantly longer.

Our simulations should be compared with true astronomical data. Below in Figure 11 it is clear that there is a qualitative match between the images produced computationally in this

project and certain interacting galaxies. Specifically, one sees the formations of bridges and *counterarms*. However, there are notable counter examples discussed in [6] and reasons such as magnetic or viscous effects have been suggested as the cause[13]. Further, our interactions were (unrealistically) restricted to a plane for simplicity, whereas real interactions will be three dimensional. This would not be difficult to implement by adapting the **Vec2** class. A collection of astronomical measurements would be required to draw further conclusions from our quantitative results.

(a) Arp 242 (b) M51 (c) Arp 87

Figure 11: Photographs of interacting galaxies from *Hubblesite*. Noticeable in these images are inter galactic bridges and counterarms. The main cause for differences, both qualitatively and quantitatively will be that our simulations are all restricted to within a plane, whereas these are three-dimensional interactions. Fortunately the object-orientated approach means that changing the **Vec2** class to a 3d representation would implement seamlessly due to the levels of abstraction. This would allow for more direct comparison with true astronomical setups.

References

[1] E. Holmberg, Atrophys.J. 92 , 200 (1940)

[2] E. Holmberg, Atrophys.J. 94 , 385 (1941)

[3] S. Tremaine,ed. S.M. Fall & D. Lynden-Bell *The structure and evolution of normal galaxies - Galaxy Mergers*, pp67-85, (1979).

[4] J.P. Ostriker, P.J.E Peebles, A. Yahil, Astrophys.J.Lett., *202*, L113

[5] A. Toomre,*The Evolution of Galaxies and Stellar Populations* ed B.M. Tinsley & R.B. Larson, p401, Yale University Press

[6] A. Toomre & J. Toomre,*Galactic Bridges and Tails* Astrophys.J. , *203* , 72

[7] S.D.M White, Mon.Not.R.Astr.Soc., *174*, 19, (1978)

[8] N. Roos & C.A. Norman, Astron.Astrophys. , *76*, 75, (1979)

[9] A. Dekel, M. Lecar & J. Shaham Astrophys.J. , *241*, 946 (1980)

[10] J.V. Villumsen, Mon.Not.R.Astr.Soc. *199* , 493, (1982)

[11] R.H. Miller & B.F. Smith Astrophys.J. *235*, 421 (1980)

[12] T. Pang, *An Introduction to Computational Physics*,Cambridge University Press, pp232-236, (2006)

[13] W. C. Saslaw, *Gravitational Physics of Stellar and Galactic Systems*, Cambridge University Press,pp466-471, (1985)

[14] G. Booch,R.Maksimchuk M. Engle ,B. Young J. Conallen, K. Houston, *Object-oriented analysis and design with applications* , Addison-Wesley Professional

[15] B.J. Cox, *Object oriented programming*, Addison-Wesley, (1985)

[16] L.S.Sparke & J.S. Gallagher, *Galaxies in the Universe: an Introduction*, p297-300, (2207)

[17] J. Binney, M. Merrifield,*Galactic astronomy*, (1998)

Appendices

Appendix A Disadvantages of the N-body Simulation and Two-Body Relaxation Effects

It was discussed in Section 2 that, although it may seem like a more accurate model, the full N-body simulation has disadvantages that makes it less useful than our model which idealises the outer disk as test masses. The obvious disadvantage is the extra computer power required to produce similar results as the efficiency of an N-body model is $\mathcal{O}(N^2)$. However, with ever increasing computer speed it is possible to attain results, although the ring density will be lower and hence the intricacies of the pattern may be lost. This means the N-body simulation is more prone to statistical fluctuations, as fewer particles must be used.

Another problem is caused by two body relaxation effects, first discussed in relation to this topic in [7]. If the stellar density of a galaxy is large, the gravitational star-star interactions deflect the trajectories the stars would have if the distribution of matter were smooth. This effect is called two-body relaxation and causes the evolution of galaxies even when they are isolated[3, 7]. This makes it difficult to tell what effects are caused by a galaxy-galaxy interaction rather than the effects of the galaxy's stellar medium upon itself. Since our outer disks are massless, we avoid this problem and an isolated galaxy does not evolve. The only disadvantage is that we lose self-gravitating effect of stellar medium.

Appendix B Derivation of Initial Conditions of Parabolic Orbits

In the simulation it is necessary to set two massive bodies in parabolic orbit with one another. For some tests conducted it was necessary to keep the parabolic orbit for a given arbitrary mass, separation and start position. The algebraic task of finding these initial conditions is given below and is coded in **void parabolicGalaxies** in **UniverseClass.cpp**.

For the orbit to have a fixed centre of mass the total momentum must be zero and the galaxies must be connected by a straight line passing through the centre of mass (set at the origin) at all times. For parabolic orbits the total energy is zero. We know that the equations for a parabolic orbit (eccentricity $e = 1$) and its derivative are given by:

$$r_1(\theta_1) = \frac{r_{0,1}}{1 + \cos(\theta_1)} \tag{6}$$

$$v_{r,1} = \frac{dr_1}{dt} = \frac{r_{0,1}\sin(\theta_1)}{(1 + \cos(\theta_1))^2}\frac{d\theta_1}{dt} \tag{7}$$

Where r_1 and θ_1 are the polar positions of the first mass, m_1, $r_{0,1}$ is the semi latus rectum, t is time and $v_{r,1}$ is the radial velocity. We can calculate $r_{0,2}$ for the second mass, m_2, using the centre of mass condition giving $r_{0,2} = -\frac{m1 r_{0,1}}{r_{0,2}}$, where we have taken a sign convention that $\theta_2 = \theta_1$. This gives us similar expressions for r_2 and $\frac{dr_2}{dt}$. The condition also gives us the initial r_2 from the initial r_1

The derivatives allows us to relate the radial and angular velocities of both bodies using $v_\theta = r1\frac{d\theta_1}{dt}$. Thus we constrain the energy as:

$$\frac{1}{2}m_1\left({v^2}_{r,1} + {v^2}_{\theta,1}\right) + \frac{1}{2}m_1\left({v^2}_{r,2} + {v^2}_{\theta,2}\right) - \frac{2Gm_1m_2}{r_1 + r_2} = 0 \tag{8}$$

and by relating velocities this simplifies to:

$$\frac{1}{2}m_1\left(\left(\frac{r_{0,1}\sin(\theta_1)}{r_1\left(1+\cos(\theta_1)\right)^2}\right)^2 + 1\right){v^2}_{\theta,1} + \frac{1}{2}m_2\left(\left(\frac{r_{0,2}\sin(\theta_1)}{r_2\left(1+\cos(\theta_1)\right)^2}\right)^2 + 1\right){v^2}_{\theta,2} - \frac{2Gm_1m_2}{r_1+r_2} = 0 \tag{9}$$

We then set $\frac{1}{2}m_1\left(\left(\frac{r_{0,1}\sin(\theta_1)}{r_1(1+\cos(\theta_1))^2}\right)^2 + 1\right) = c_1$ and $\frac{1}{2}m_2\left(\left(\frac{r_{0,2}\sin(\theta_1)}{r_2(1+\cos(\theta_1))^2}\right)^2 + 1\right) = c_2$ and $\frac{2Gm_1m_2}{r_1+r_2} = c_3$. Then, the condition for zero net momentum becomes $v_{\theta,2} = c_4 v_{\theta,1}$ with $c_4 = \frac{m2}{m1}$ and we can solve simultaneously for $v_{\theta,2}$ and $v_{\theta,1}$ to give:

$$v_{\theta,2} = \frac{\sqrt{c_3}c_4}{\sqrt{c_1 + c_2{c_4}^2}}, v_{\theta,1} = \frac{\sqrt{c_3}}{\sqrt{c_1 + c_2{c_4}^2}} \tag{10}$$

from which the initial radial velocities may be trivially calculated using Equation 7. In the case of $m1 = m2$ there is great simplification due to the symmetry and the magnitudes of velocities will be the same for each mass:

$$v_\theta = \frac{1}{2}\sqrt{\frac{Gm}{r_0}}(1+\cos(\theta)), v_r = \frac{1}{2}\sqrt{\frac{Gm}{r_0}}\sin(\theta) \tag{11}$$

Appendix C Code Listing

Please email timothy.harrison@cantab.net if you would like to obtain a copy of the code used to perform this investigation.